On a toroidal method to solve the sessile drop oscillation problem

Saksham Sharma† and D. Ian Wilson

Department of Chemical Engineering and Biotechnology, University of Cambridge, Philippa Fawcett Drive, Cambridge CB3 0AS, UK

(Received xx; revised xx; accepted xx)

We present a fully analytical solution for the natural oscillation of an inviscid sessile drop with small Bond number (surface tension dominates gravity) and a fixed contact line on a flat horizontal plate. The governing equations are expressed in terms of the toroidal coordinate system which yields solutions involving *hypergeometric functions*. Resonant frequencies are identified for zonal, sectoral and tesseral vibration modes. The predictions show excellent agreement with experimental data reported in the literature, particularly for flatter drops (lower θ_c, but not so low as to incur significant viscous dissipation) and higher modes of vibration.

Key words: Inviscid, Laplace, sessile drop, toroidal coordinates

1. Introduction

The study of natural oscillations of a drop dates back over a century to the seminal work of Rayleigh (1879), who found analytical expressions for oscillation frequencies of an inviscid, spherical, free drop. Lamb (1932) extended the analysis to include azimuthal mode shapes, using spherical harmonics $Y_l^m(\theta, \varphi)$ of degree l and order m. Chandrasekhar (1959) subsequently considered the contribution of viscosity to explain the damping in a viscous drop. Other studies in this area have included the effects of (i) viscosity, such as those of Miller & Scriven (1968) and Prosperetti (1980), and (ii) moderate-amplitude oscillations, such as Tsamopoulos & Brown (1983).

In recent times research in this area has shifted from the case of a free drop to a pendant drop supported on a solid rod, e.g. Wilkes and Basaran (see Wilkes & Basaran (1994), Wilkes & Basaran (1997) and Wilkes & Basaran (2001)). The case of the sessile drop has been studied by many, for example Lyubimov *et al.* (2006), who considered natural oscillations of a hemispherical, inviscid drop. While the free drop is generally assumed to be spherical, a sessile drop takes the form of a spherical cap when surface tension dominates gravity (i.e. $\sqrt{\gamma/\rho g} >> c$, where γ is the surface tension, ρ is the density and c is the contact radius of the drop). To find natural frequencies of the latter, analytical models in the literature either converted the geometry to a simplified form (replacing the planar substrate by a spherical one, Strani & Sabetta (1984)) or developed a solution using spherical coordinates (Bostwick & Steen (2014)). While the former approach leads to a highly simplified physical model, the latter requires hybrid analytical-numerical schemes: neither is then suitably accurate and accessible for use by an experimentalist.

Bostwick and Steen (Bostwick & Steen (2016), Steen *et al.* (2016)) have presented a

† Email address for correspondence: ss2531@cam.ac.uk

detail account of the underlying physics and mechanics of this problem. The contact angle θ_c (and shape) of the drop is established at static equilibrium by balancing the liquid/gas, liquid/solid and solid/gas interfacial tensions. The drop stability is determined by the contact line (CL) behaviour, via its speed u_{CL}. Stick-slip behaviour of the CL (Shaikeea *et al.* (2017)) gives rise to hysteresis, which is captured using a CL model. In the "Hocking condition" presented by Davis (1980), contact-angle deviations are expressed in the form $\Delta\theta_c \propto u_{\mathrm{CL}}$, with a constant of proportionality Λ which quantifies the CL resistance. This phenomenological parameter characterises the CL mobility; $\Lambda = 0$ corresponds to a fully mobile CL and $\Lambda = \infty$ to a pinned CL. In the current work, the toroidal framework imposes the pinned CL condition on the problem (see §2.4.).

We present here an analytical solution to this long-standing problem by using a toroidal coordinate system. The fluid-vapour and fluid-solid boundaries of a spherical cap, δD_f and δD_s (cf. Fig. 1(a)), correspond to a pair of β-coordinate curves in this system, where the boundary conditions can be directly expressed, without any geometric conversions or complex computations. Solving hydrodynamics equations in this framework requires the use of *hypergeometric functions*, which ultimately yields a fully analytical solution in the form of Eq. (2.18). The importance of chosing this framework to solve the sessile drop evaporation problem was first presented by Popov (2005) and we believe this is the first time it has been extended to the oscillating sessile drop.

Bostwick & Steen (2014) (hereafter referred to as Bo-St) presented a hybrid analytical-numerical model which solves the same problem and employs inverse operators to find the solution. Theirs is the most comprehensive investigation of the sessile drop oscillation problem to date. They considered different types of vibration mode shapes, namely zonal, sectoral and tesseral, which were subsequently validated experimentally by Chang *et al.* (2015). In the current work, the resonant frequencies for the mode shapes discussed by Bo-St are calculated and compared with the experimental data reported in literature.

The purpose of this work is to show that our model based on toroidal coordinates yields fully analytical solutions for the case of an inviscid drop with fixed contact line in the shape of a spherical cap. Stating the hydrodynamic equations with boundary conditions, we perform an eigenmode analysis to find the solution (§2). This model is then used to identify resonant frequencies for zonal, sectoral, and tesseral vibration modes (§3). Its predictions are compared with experimental data reported in the literature. Future work and possible extensions of this model have been discussed in (§4).

2. Theory

2.1. *Sessile drop geometry*

The fluid-vapour interface of a sessile drop with contact angle $\theta_c \in (0, \pi)$ can be expressed in toroidal coordinates as $\mathbf{r}' = \mathbf{r}'(\alpha, \beta, \varphi)$ (Fig. 1(a)). Variable $\alpha \in [0, \infty)$ varies along the surface ∂D_f, where $\beta \in [0, \pi]$ is the angle subtended by foci F_1, F_2 on ∂D_f and $\varphi \in [0, 2\pi]$ varies in the azimuthal direction. The equilibrium (base) state Γ of the drop can be defined as

$$\beta = \beta_0, \quad \alpha \in [0, \infty], \quad \varphi \in [0, 2\pi] \tag{2.1}$$

A small perturbation $\eta'(\alpha, \varphi, t)$ on Γ (with the contact line being fixed) leads to a competition between drop's inertia and capillarity, and the resulting motion is oscillatory in nature (cf. Fig. 1b). These disturbances are often expressed in terms of

$$h'_\alpha = h'_\beta = \frac{c}{\cosh\alpha - \cos\beta}, h'_\varphi = \frac{c \sinh\varphi}{\cosh\alpha - \cos\beta} \tag{2.2}$$

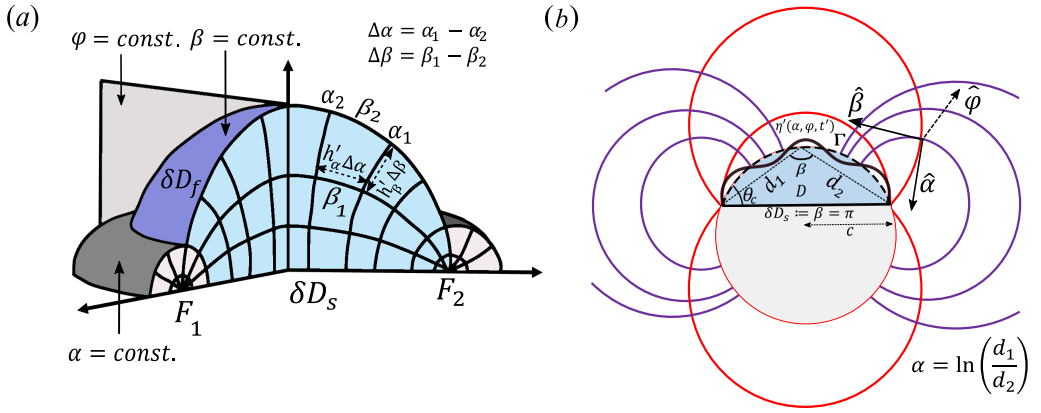

Figure 1: (a) 3D schematic of toroidal coordinate system $\mathbf{r}' = \mathbf{r}'(\alpha, \beta, \varphi)$ overlaid on a sessile drop. Based on Li & Kumar (2019). (b) Diametral section of the drop (blue shaded region) with toroidal gridlines embedded into it. On a red circle, β is constant, and on a purple circle, α is constant. Defining expressions for α and β are also displayed.

where c is the drop contact radius and h'_α, h'_β and h'_φ are the scale factors of the toroidal system. Here the prime notation indicates that the variables are dimensional. In the following text, prime notations will be dropped to express dimensionless variables; except for density ρ, surface tension γ, and contact radius c of the drop. The scale factor quantifies the change in position of a point on changing one of its coordinates, so a $\Delta\alpha$ change in α (keeping other coordinates constant) corresponds to a change in distance along $\hat{\alpha}$ of $h'_\alpha \Delta\alpha$ (cf. Fig. 1(a)).

2.2. *Equations and boundary conditions*

The flow is assumed to be incompressible and irrotational. The velocity field $\mathbf{v}'$ is described as $\mathbf{v}' = \nabla\psi'$, where the velocity potential ψ' satisfies Laplace's equation

$$\nabla^2\psi' = 0 \quad [D] \tag{2.3}$$

in the drop domain D. The equation becomes closed form when subject to the no-penetration condition

$$\nabla\psi' \cdot \boldsymbol{\beta} = \frac{1}{h'_\beta}\frac{\partial\psi'}{\partial\beta} = 0 \quad [\partial D_s := \beta = \pi] \tag{2.4}$$

at the substrate ∂D^s and a free-surface kinematic boundary condition

$$\nabla\psi' \cdot \boldsymbol{\beta} = \frac{1}{h'_\beta}\frac{\partial\psi'}{\partial\beta} = \frac{\partial\eta'}{\partial t'} \quad [\partial D_f := \beta = \pi - \theta_c] \tag{2.5}$$

at the interface ∂D_f, where the normal velocity is equalized to the time-derivative of perturbation. For an inviscid fluid, applying linear wave theory, the pressure field is described by the momentum equation

$$p' = -\rho\frac{\partial\psi'}{\partial t'} \quad [D] \tag{2.6}$$

A small disturbance η' to the equilibrium surface Γ causes a deviation from the initially spherical shape which is described by the modified Laplace equation

$$\frac{p'}{\gamma} = -(k_1^2 + k_2^2)\eta' - \Delta_T \eta' \tag{2.7}$$

where k_1, k_2 are the principal curvatures, Δ_T is the Laplace-Beltrami operator, and definitions are given in Appendix A. In subsequent sections, we have replaced the term $\cosh\alpha - \cos\beta$ with $b(\alpha,\beta)$ while simplifying the terms involving scale factors h'_α, h'_β and h'_φ.

2.3. *Curvatures and Laplace-Beltrami operator for toroidal coordinates*

The first and second fundamental forms of a surface allow the calculation of curvature and Laplace-Beltrami operators, respectively, for a parametric surface $\mathbf{x}(u^1, u^2)$. The coefficients for first fundamental form are given by the metric tensor

$$g_{ij} \equiv \mathbf{x}_i \cdot \mathbf{x}_j = \begin{pmatrix} E & F \\ F & G \end{pmatrix} \tag{2.8}$$

where $\mathbf{x}_i = \frac{\partial \mathbf{x}}{\partial u^i}$, $\mathbf{x}_j = \frac{\partial \mathbf{x}}{\partial u^j}$ and $i, j = 1, 2$ (Kreyszig (1959)). The derivation of the principal curvatures and the Laplace-Beltrami operator from the coefficients E, F and G is given in Appendix A.

2.4. *Reduction to eigenmode problem*

The characteristic length scale assumed in this problem is the contact radius of the drop, c. Performing a dimensional analysis on the 6 parameters; $p', \psi', t', \rho, \gamma$ and c (or equivalently η') involved in Eq. (2.6)-(2.7) gives rise to 3 dimensionless parameters: $\frac{\psi' t'}{c^2}$, $\frac{\gamma t'^2}{\rho c^3}$ and $\frac{p' t'^2}{\rho c^2}$, giving characteristic scalings of $\sqrt{\frac{\rho c^3}{\gamma}}$ (time), $\sqrt{\frac{\gamma}{\rho c}}$ (velocity) and $\frac{\gamma}{c}$ (pressure).

A drop with pinned contact line is subjected to a small perturbation $\eta'(\alpha, \varphi, t)$. Resolving dimensional η' and ψ' into individual components (Drazin (2002)): dimensionless eigenfunctions $y(\alpha)$ and $\phi(\beta, \alpha)$, normal modes (frequency Ω), and azimuthal direction (wavenumber l), gives

$$\eta'(\alpha, \varphi, t') = c\, y(\alpha) e^{i\Omega' t'} e^{il\varphi}, \quad \psi'(\mathbf{r}', t') = \sqrt{\frac{\gamma c}{\rho}}\, \phi(\beta, \alpha) e^{i\Omega' t'} e^{il\varphi} \tag{2.9}$$

Substituting Eq. (2.9) into Eq. (2.3)-(2.7) yields

$$\frac{\partial}{\partial \beta}\left(h_\varphi \frac{\partial \phi}{\partial \beta}\right) + \frac{\partial}{\partial \alpha}\left(h_\varphi \frac{\partial \phi}{\partial \alpha}\right) - \frac{l^2}{b(\alpha,\beta)\sinh\alpha}\phi = 0 \quad [D] \tag{2.10a}$$

$$\frac{\partial \phi}{\partial \beta} = 0 \quad [\partial D_s := \beta = \pi] \tag{2.10b}$$

$$\frac{\partial \phi}{\partial \beta} = \frac{i\lambda y}{b(\alpha, \beta_0)} \quad [\partial D_f := \beta = \pi - \theta_c] \tag{2.10c}$$

$$i\lambda\phi = 2\sin^2\beta y + b^2(\alpha, \beta_0)\left[\frac{1}{\sinh\alpha}\frac{\partial}{\partial\alpha}\Big(\sinh\alpha \frac{\partial y}{\partial \alpha}\Big) - \frac{l^2 y}{\sinh^2\alpha}\right] \tag{2.10d}$$

$$\lambda^2 = \frac{\rho \Omega'^2 c^3}{\gamma} \tag{2.10e}$$

where $b(\alpha,\beta_0)$ means that it is defined on the interface $\Gamma := \beta = \beta_0$. Eq. (2.10$a$) is Laplace's equation in separated form, Eq. (2.10b) is the no-penetration boundary condition, Eq. (2.10c)-(2.10d) are free surface kinematic boundary conditions and Eq. (2.10e) gives the dimensionless frequency λ. It is to be noted that all variables in Eq. (2.10a)-(2.10d) are dimensionless, hence without prime notations.

2.5. *Solving the eigenmode equations*

The solution to Eq. (2.10a) in the toroidal system is given by Lebedev (1965) as

$$\phi = a\left[AP^l_{v-\frac{1}{2}}(\cosh\alpha) + BQ^l_{v-\frac{1}{2}}(\cosh\alpha)\right][C\cos v\beta + D\sin v\beta] \tag{2.11}$$

where $a = \sqrt{2(\cosh\alpha - \cos\beta)}$, $P^l_{v-\frac{1}{2}}(\cosh\alpha)$ and $Q^l_{v-\frac{1}{2}}(\cosh\alpha)$ are Legendre functions of the first and second kind (also called toroidal functions) with v the toroidal degree and l the azimuthal order. At $\alpha = 0$, $P^l_v(1) = 1$ and $\lim_{z\to 1+} Q^l_v(z) = \infty$, which means that the latter is not defined at the apex of the drop. Thus, setting $B = 0$ and $v = i\tau$ (see Lebedev 1965, p. 227) gives

$$\phi = aP^l_{i\tau-\frac{1}{2}}(\cosh\alpha)[C\cos i\tau\beta + D\sin i\tau\beta] \tag{2.12}$$

Using Eq. (2.10) and substituting $\beta = \pi$ in Eq. (2.10b) gives $C = -iD\coth\pi$. Upon further simplification, Eq. (2.12) reduces to

$$\phi = aP(\cosh\alpha)f(\tau\beta) \tag{2.13}$$

where $P(\cosh\alpha)$ denotes $P^l_{i\tau-1/2}(\cosh\alpha)$ and $f(\tau\beta) = \sinh\tau\beta - \coth\tau\pi\cosh\tau\beta$. Substituting Eq. (2.13) in Eq. (2.10c) (after multiplying its both sides by $b(\alpha,\beta_0)$) gives

$$i\lambda y = b(\alpha,\beta_0)\frac{\partial\phi}{\partial\beta} = P\,b(\alpha,\beta_0)\left(\frac{f}{a}\sin\beta_0 + \tau a f_1\right) = PT \tag{2.14}$$

where $T(\alpha,\beta_0) = b(\alpha,\beta_0)(\frac{f}{a}\sin\beta_0 + \tau a f_1)$ and $f_1 = \cosh\tau\beta_0 - \coth\tau\pi\sinh\tau\beta_0$. Functions $T(\alpha,\beta_0)$, $f(\tau\beta_0)$, $f_1(\tau\beta_0)$ and $P(\cosh\alpha)$ are written without arguments for clarity.

An important consequence of Eq. (2.14) is that $y = 0$ at the contact line, which arises because $P \to 0$ as $\alpha \to \infty$: the use of the toroidal coordinate system imposes the fixed contact-line condition on the problem. The mobility of the contact-line is defined as $1/\Lambda$ by Bo-St, which is zero for an immobile contact-line and infinite for a fully mobile contact-line. Only the immobile contact-line case, $\Lambda = 0$, is considered in the current work.

Substituting the above equation in Eq. (2.10d) gives, at $\beta = \beta_0$;

$$-\lambda^2\phi = 2\sin^2\beta_0 PT + b^2(\alpha,\beta_0)\left[\frac{1}{\sinh\alpha}\frac{\partial}{\partial\alpha}\left(\sinh\alpha\frac{\partial}{\partial\alpha}(PT)\right) - \frac{l^2}{\sinh^2\alpha}PT\right] \tag{2.15}$$

This can be re-arranged to

$$-\lambda^2\phi = 2\sin^2\beta_0 PT + b^2(\alpha,\beta_0)[IT + II] \tag{2.16}$$

where I and II are, respectively,

$$I = \frac{1}{\sinh\alpha}\frac{\partial}{\partial\alpha}\left(\sinh\alpha\frac{\partial P}{\partial\alpha}\right) - \frac{l^2}{\sinh^2\alpha}P \tag{2.17a}$$

$$II = \frac{\partial T}{\partial\alpha}\frac{\partial P}{\partial\alpha} + \frac{1}{\sinh\alpha}\frac{\partial}{\partial\alpha}\left(\sinh\alpha\,P\frac{\partial T}{\partial\alpha}\right) \tag{2.17b}$$

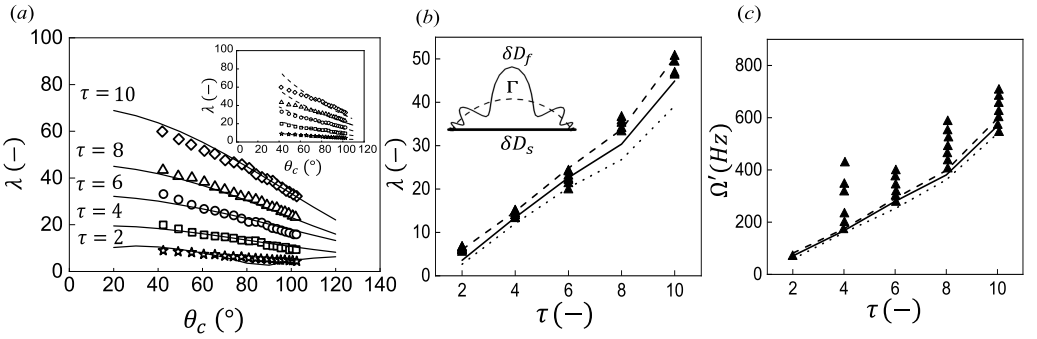

Figure 2: Results for zonal modes, $m = 0$. (a) Effect of contact angle θ_c on dimensionless frequency λ for toroidal mode number τ. Solid lines are solutions to Eq. (2.18) and symbols are the experimental values reported by Chang *et al.* (2015). Inset shows the comparison of same experiments with Bo-St model (dashed lines). (b and c) Effect of τ on λ and Ω'. Symbols show experimental values reported by (b) Chang *et al.* (2013) and (c) Mettu & Chaudhury (2012) for a water drop. Loci show model predictions for different contact angles: (b) solid line, $\theta_c = 68.6°$; dashes, $\theta_c = 63.6°$; dots, $\theta_c = 73.6°$. (c) solid line, $\theta_c = 79.5°$; dashes, $\theta_c = 68°$; dots, $\theta_c = 91°$. Inset in (b) shows interface shape y plotted on Γ using Eq. (2.18) for $\tau = 10$ (not to scale).

The term I is equivalent to $(v^2 - \frac{1}{4})P$ (see Lebedev 1965, p. 224). In fact, an analogous simplification is performed while deriving an expression for the eigenfrequencies of a free spherical drop in Rayleigh's derivation, (see Landau & Lifshitz. 1987, p. 246). Further simplification of the RHS of Eq. (2.16) gives

$$-\lambda^2 = \left[2\sin^2\beta_0 - b^2(\alpha,\beta_0)\left(\tau^2 + \frac{1}{4}\right)\right]\frac{T}{af} + \frac{b^2(\alpha,\beta_0)}{af}\left[T_\alpha\left(\frac{2P_\alpha}{P} + \coth\alpha\right) + T_{\alpha\alpha}\right] \quad (2.18)$$

where a single or double subscript α on a function denotes single or double derivative of the function w.r.t. α. The expressions for $T_\alpha, T_{\alpha\alpha}, P$ and P_α (which fall under the class of *hypergeometric functions*) are given in Appendix B.

3. Results

The variation of dimensionless frequency λ with contact angle $\theta_c = \pi - \beta_0$ is determined by solving (2.18). Previous studies such as Bo-St classified the vibrational modes as zonal ($l = 0$), sectoral ($\tau = l$) and tesseral ($l \neq 0, \tau \neq l$). Results are presented for each type of mode in turn.

3.1. *Zonal ($l = 0$) modes*

When the disturbance of the interface is axisymmetric, the mode shapes are termed zonal. For a sessile drop of fixed contact radius c, increasing the contact angle θ_c increases the volume of drop (inertia) and thus decreases the frequency λ (cf. Fig. 2(a)). There is excellent agreement between the model and the data of Chang *et al.* (2015) in this Figure, particularly at higher mode numbers. For instance, for $\tau = 10$ and $\theta_c = 40°$, our model overpredicts slightly, by a factor of 1.05, while the Bo-St model overpredicts by a factor of 1.25 (see inset Fig. 2(a)). For the other modes at $\theta_c < 60°$, the agreement is better than the Bo-St model. Higher mode numbers correspond to more points (nodes) of intersection of the disturbed interface δD_f with the undisturbed interface Γ. Since there

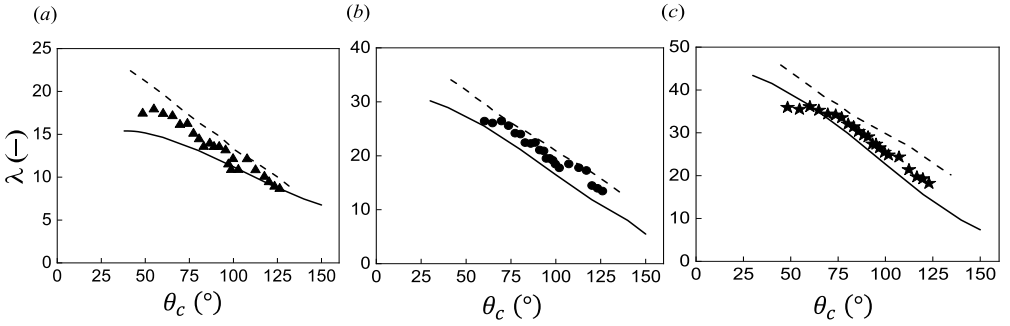

Figure 3: Effect of contact angle on dimensionless frequency for sectoral modes, $\tau = l$, for (a) [5,5], (b) [7,7], (c) [9,9]. Solid loci show the solutions to (2.18)), dashed loci are the results presented by Bostwick & Steen (2014). Symbols indicate experimental data reported by Chang *et al.* (2015).

is no variation in the azimuthal direction, a front view (see inset Fig. 2(b)) is sufficient to describe the mode shape. This Figure shows the case with 10 nodes ($\tau = 10$).

Further comparisons of predicted zonal mode frequencies with experimental measurements are shown for the data sets reported by Chang *et al.* (2013) and Mettu & Chaudhury (2012) in Fig. 2(b) and Fig. 2(c), respectively. In the former, the experimental values lie within the range of theoretical frequencies calculated for the range of contact angles θ_c involved. For the higher modes, $\tau = 8$ and 10, the frequencies lie at the upper end of the theoretical span, where there were a limited number of data points as these require larger droplets ($\gtrsim 5\mu L$ (see Mettu & Chaudhury 2012, Fig.4(a))), whereas lower modes ($\tau = 2, 4, 6$) were experimentally accessible for droplets with smaller volume, $\leq 5\mu L$. Also, there is a small increase in slope at $\tau = 8$ (due to frequency at $\tau = 10$) which is apparent in Fig. 2(a), in the form of slight over-prediction of the model, at $\tau = 10$, for $\theta_c \approx 65°$. In Fig. 2(c), the width of the predicted frequency band is small and lies at the lower end of the range of observed frequencies. A possible explanation for this mismatch is that the model neglects contributions from viscous effects. Chang *et al.* (2013) reported that the bandwidth of predicted frequencies increased when viscous contributions were added (noting that the dimensional frequency is plotted here). Chang *et al.* (2015) subsequently showed that the viscous contribution is characterised by the Ohnesorge number, $Oh = \mu/\sqrt{\rho c \gamma}$, and even at a small value of $Oh = 0.003$ for water (instead of $Oh = 0$ for the inviscid case) the resonant peak changed from an infinite to a finite value and thus increased the bandwidth of predicted frequency (see Chang *et al.* (2015, p. 446)). The effect of viscosity on a drop undergoing oscillations of arbitrary amplitude has been discussed both for free drops and sessile/pendant drops (see Basaran (1992) and Wilkes & Basaran (1997)). For the latter case, it has been reported that as the viscosity increases, the resonant frequency also increases, so that excluding viscous effects can lead to predicted frequencies lying at the lower end of the observed spectrum.

3.2. *Sectoral ($\tau = l, l \neq 0$) modes*

A non-axisymmetric mode with wavenumber pair $[\tau, l]$ has l longitudinal intersections and $(\tau - l)/2$ latitudinal intersections (or $\tau - l$ nodes on the interface) with the undisturbed interface Γ (see Bostwick & Steen 2014, p. 19). A sectoral mode, with $\tau = l$, is a special case where there are only longitudinal intersections. Fig. 3 compares the experimental frequencies reported by Chang *et al.* (2015) with our model and the Bo-St model. There

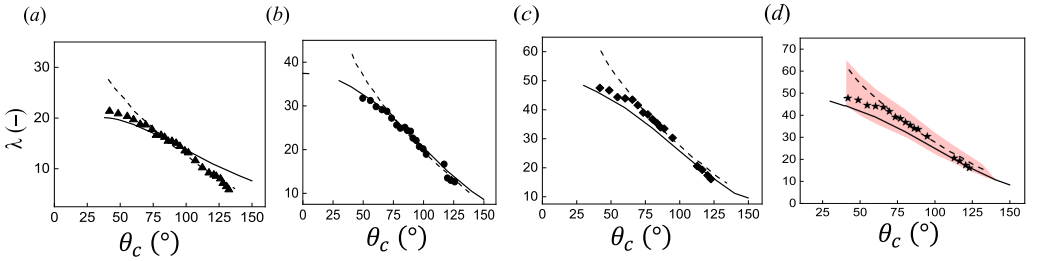

Figure 4: Effect of contact angle on dimensionless frequencies for tesseral modes with $[\tau, m]$ values of (a) [5,3], (b) [7,5], (c) [9,5] and (d) [9,7]. Solid loci show the solutions to Eq. (2.18)), dashed lines are the results presented by Bostwick & Steen (2014). Symbols show experimental data reported by Chang *et al.* (2015). The shaded region in panel (d) represents the range of frequencies calculated using VPF theory by Chang *et al.* (2015) for water, with substrate forcing and viscosity included.

is a good agreement with our model for $\tau = 9$. For $\tau = 5$ and 7, the two models bracket the data.

3.3. *Tesseral ($\tau \neq l, l \neq 0$) modes*

A tesseral mode shape with wavenumber pair $[\tau, l]$ has non-zero longitudinal and latitudinal intersections because $\tau \neq l$. Fig. 4 compares the results for our model and the Bo-St model in a similar fashion to the sectoral mode. For the $\tau = 9$ cases, our model agrees with the experimental data quite well for all θ_c values investigated. For $\theta_c \leq 65°$, the Bo-St model does not capture the observed trend: for 50° and $l = 7$, it overpredicts by a factor of 1.17 while our model underpredicts slightly by a factor of 1.05. For $\tau = 7$, there is good agreement between the experimental data and both models as θ_c decreases from 140° to 70°, below which our model continues to perform well and Bo-St starts to diverge. For $\tau = 5$, our model captures the frequencies at low θ_c while the Bo-St model works well at higher values.

It should be noted that our model cannot predict the frequencies for small contact angles, because in this case a larger fraction of the sessile drop volume lies within the solid/liquid boundary layer: drop-substrate interactions then cause damping of oscillations. The range of contact angles suggested to avoid boundary layer viscous dissipation effects, discussed in Sharp (2012), is 30° – 150°.

For the lowest mode, [5,3], there is a slight over-prediction for larger contact angles. This can be attributed to the assumption of a pinned contact line in the current work. If the contact line is, instead, assumed to be mobile and not pinned, the slope of frequency versus contact angle curve will decrease at larger contact angles (see Bostwick & Steen 2014, Fig. 10 and 11). This represents a limitation in the current model in that mobile contact line behaviour is not readily incorporated in the toroidal coordinate approach.

4. Discussion and conclusions

The superior performance of our model for lower θ_c and higher modes is likely the result of using toroidal coordinates, which fit the sessile drop naturally. An interesting physical insight from this work is that the slope of λ *vs.* θ_c curve decreases as the θ_c decreases; the curve almost reaching a plateau. It is suggested by experiments as well. The physical models present in literature incorporated bulk dissipation and contact-line (Davis) dissipation, e.g. Bostwick & Steen (2016), to account for this plateau. On the

other hand, the current toroidal model, while established on zero viscosity and fixed contact-line assumptions, can still predict this plateau with good success. While on one hand, incorporating more dissipation terms will improve this model and bring more understanding of observations such as mode-mixing and mode-competition (Bostwick & Steen (2015)). On the other hand, the strength of this inviscid theory coupled with an appropriate coordinate system points to the importance of choosing a framework which maps the complicated geometries of physics problems perfectly, as previously done in Fokas & Nachbin (2012), Richardson (1992).

There are exceptions, e.g. Fig. 3(a), 4(a), and we here consider whether the mismatch between the predictions of the model and the experimental data could arise from the assumptions made in our model. The larger error incurred by the Bo-St model can be attributed to the approach used to enforce the no-penetration condition. Earlier works on constrained drops (e.g. Ramalingam *et al.* (2012) and Prosperetti (2012)) essentially used the Lagrange multiplier method to enforce the no-penetration condition at the pinning circle and these methods permitted a discontinuity in the interface shape at the contact point. The Bo-St method does not allow a discontinuity at the pinning sites, which leads to overprediction of the frequency (see Bostwick & Steen 2015, p. 558).

The model considers the sessile drop on a substrate as a mass-spring system, where viscous effects and substrate-drop interactions are neglected. These assumptions were also made in the Bo-St model and were subsequently relaxed in their subsequent work, for example, Bostwick & Steen (2016), where they studied damping for viscous drops (with fixed contact-line) undergoing substrate-forced oscillation. To extend our model along the lines discussed in Chang *et al.* (2015), viscous contributions could be incorporated by adding a damping term, $i\lambda\epsilon C[y]$, to the RHS of (2.15), where C is the dissipation operator and $\epsilon = \frac{\mu}{(\rho c \gamma)^{1/2}}$ is the Ohnesorge number. Substrate-drop interactions can be modeled using two main assumptions: (i) constant contact radius, and (ii) modeling the substrate-forcing via the bulk pressure in the drop in the form of Faraday oscillations. With regard to (i) it should be noted that contact angle hysteresis on the modes cannot be incorporated using the toroidal framework presented here because it requires the incorporation of a dynamic contact-line condition (Bostwick & Steen (2014)). With (ii), the substrate contribution is incorporated by adding a term $F_0 e^{i\lambda t}$ to the RHS of Eq. (2.15), where λ is the frequency of substrate forcing (not the natural frequency) and F_0 its amplitude. Chang *et al.* (2015) used these assumptions and incorporated the aforementioned effects in their VPF (viscous potential flow) theory. The envelope of solutions which they obtained is shown as a shaded region in Fig. 4(d) and it spans Bo-St and our model (both inviscid). It is, thus, expected that the addition of viscous and substrate contributions to our model will modify Eq. (2.18) and increase the bandwidth of predicted frequencies. This is the subject of ongoing work, where the aim is to identify the contributions of viscous damping and substrate forcing, and thereby establish when significant differences will arise from the inviscid model.

The description of an oscillating drop presented here is not suitable for cases where the drop shape is influenced by gravity, which is quantified by Bo (ratio of gravity to surface tension). As the volume of the drop increases, the drop shape changes from that of a truncated sphere ($Bo = 0$), towards being ellipsoidal ($0 < Bo < 5$) until it forms a flat puddle ($Bo > 5$), with uniform depth except near the edges (Lubarda & Talke (2011)). We believe that it should be possible to model a flattened drop using confocal ellipsoidal coordinates system in the $0.5 < Bo < 5$ regime. Finding resonant frequencies for a flattened drop will allow us to extend our $Bo = 0$ theory to $0 < Bo < 5$, and compare the results with the theory for flattened drops presented by Noblin *et al.* (2004) where

the drop is modelled as a liquid bath and the resonant frequency is that associated with a standing wave on its interface.

This work introduces, for the first time, an analytical solution to the sessile drop oscillation problem. The superiority of this model lies in the fact that its predictions work well for lower contact angles ($< 75°$) compared to the existing models. It also predicts a decrease in slope as θ_c decreases, which is consistent with experiments. The behaviour at lower contact angles ($< 30°$) remains to be experimentally validated (and physically understood) for all types of modes.

To summarise, our model provides a concise solution to the sessile drop oscillation problem which opens a new window to the researchers interested in this and related problems. A clear next step could be to test the $\theta_c < 30°$ regime experimentally, model a drop being vibrated on an inclined plane (see Brunet & J. Deegan (2007)) and extend the model to larger drops by including the effects of gravity.

Acknowledgements

We wish to thank Dr. R.K. Bhagat for fruitful discussions on this problem. S.S. also benefitted greatly from insights provided by Dr. H. Tankasala and A.J.D. Shaikeea. We would like to thank an anonymous reviewer for greatly helping in improving the mathematical presentation of this work.

Funding

S.S. was funded by the Cambridge India Ramanujan Scholarship from the Cambridge Commonwealth, European and International Trust and SERB, Govt. of India.

Declaration of interests

The authors report no conflict of interest.

Appendix A. Differential geometry of toroidal system

A general point on the surface $\beta = \beta_0$ is $\mathbf{x}(\alpha, \varphi) = (x, y, z)$ such that

$$x = \frac{c \sinh\alpha \cos\varphi}{b}, y = \frac{c \sinh\alpha \sin\varphi}{b}, z = \frac{c \sin\beta}{b} \tag{A 1}$$

where $b = b(\alpha, \beta) = \cosh\alpha - \cos\beta$ (see Lebedev 1965, p. 222). Putting $i = \alpha$, $j = \varphi$ in Eq. (2.8) gives

$$\begin{aligned}
\mathbf{x}_\alpha &= \left(\tfrac{c\cos\varphi\, d}{b^2}, \tfrac{c\sin\varphi\, d}{b^2}, -\tfrac{c\sin\beta\,\sinh\alpha}{b^2}\right)\\
\mathbf{x}_\varphi &= \left(\tfrac{-c\sinh\alpha\,\sin\varphi}{b}, \tfrac{c\sinh\alpha\cos\varphi}{b}, 0\right)\\
E &= \mathbf{x}_\alpha \cdot \mathbf{x}_\alpha = \left(\frac{c}{b}\right)^2\\
F &= \mathbf{x}_\alpha \cdot \mathbf{x}_\varphi = 0\\
G &= \mathbf{x}_\varphi \cdot \mathbf{x}_\varphi = \left(\frac{c\sinh\alpha}{b}\right)^2\\
W &= \sqrt{EG - F^2} = \frac{c^2 \sinh\alpha}{b^2}
\end{aligned} \tag{A 2}$$

where $d = 1 - \cosh\alpha\cos\beta$ and W is the determinant of the metric tensor.

The coefficients of second fundamental form of surface are: $L = \mathbf{x}_{ii}\cdot\mathbf{n}$, $M = \mathbf{x}_{ij}\cdot\mathbf{n}$, $N = \mathbf{x}_{jj}\cdot\mathbf{n}$ where $\mathbf{n} = \frac{\mathbf{x}_i\times\mathbf{x}_j}{|\mathbf{x}_i\times\mathbf{x}_j|}$ and $|\mathbf{x}_i\times\mathbf{x}_j| = W$. Again, setting $i = \alpha$, $j = \varphi$ gives

$$\begin{aligned} L &= \frac{(\mathbf{x}_{\alpha\alpha}\mathbf{x}_\alpha\mathbf{x}_\varphi)}{W} = \frac{-c\sin\beta}{b^2} \\ M &= \frac{(\mathbf{x}_{\alpha\varphi}\mathbf{x}_\alpha\mathbf{x}_\varphi)}{W} = 0 \\ N &= \frac{(\mathbf{x}_{\varphi\varphi}\mathbf{x}_\alpha\mathbf{x}_\varphi)}{W} = \frac{-c\sin\beta\sinh^2\alpha}{b^2} \end{aligned} \tag{A 3}$$

where the notation $(\mathbf{a}\,\mathbf{b}\,\mathbf{c})$, used in Kreyszig (1959), stands for the triple product $\mathbf{a}\cdot(\mathbf{b}\times\mathbf{c})$ of vectors $\mathbf{a}$, $\mathbf{b}$ and $\mathbf{c}$. In Eq. (2.7), the first term in RHS is then

$$k_1^2 + k_2^2 = \left(\frac{EN - 2FM + GL}{W^2}\right)^2 - 2\frac{LN - M^2}{W^2} = \frac{2\sin^2\beta}{c^2} \tag{A 4}$$

and second term (the Laplace-Beltrami operator) becomes

$$\begin{aligned} \Delta_T\eta &= \frac{1}{W}\left[\frac{\partial}{\partial\alpha}\left(\frac{G\eta_\alpha - F\eta_\varphi}{W}\right) + \frac{\partial}{\partial\varphi}\left(\frac{E\eta_\varphi - F\eta_\alpha}{W}\right)\right] \\ &= \frac{b^2}{c^2}\Big[\frac{1}{\sinh\alpha}\frac{\partial}{\partial\alpha}\big(\sinh\alpha\frac{\partial\eta}{\partial\alpha}\big) + \frac{1}{\sinh^2\alpha}\frac{\partial}{\partial\varphi}\big(\frac{\partial\eta}{\partial\varphi}\big)\Big]. \end{aligned} \tag{A 5}$$

Another form of Eq. (A 5) is derived in the notes of Deserno (2004, p. 24).

Appendix B. Hypergeometric functions

Hypergeometric functions are solutions to the second order ODE encountered while using a system of orthogonal curvilinear coordinates to solve Laplace's equation (see Lebedev 1965, p. 161-173). In our case, we use toroidal system to solve Laplace's equation and find Legendre functions of the first kind $P_v(z)$ as the solution (hence, referred to as the toroidal functions). The integral representations of these functions are given below, for different cases:

(i) When $l = 0$ (see Lebedev 1965, p. 173)

$$P_v(\cosh\alpha) = A_1\int_0^\infty \frac{\cosh(v+\frac{1}{2})\theta}{\sqrt{2\cosh\theta + 2\cosh\alpha}}\,d\theta \tag{B 1}$$

for $\alpha > 0, -1 < Re(v) < 0$ and

$$P_\alpha = \frac{d}{d\alpha}(P_v(\cosh\alpha)) = A_1\sinh\alpha\int_0^\infty \frac{-\cosh(v+\frac{1}{2})\theta}{(2\cosh\theta + 2\cosh\alpha)^{\frac{3}{2}}}\,d\theta \tag{B 2}$$

for $\alpha > 0, -1 < Re(v) < 0$. $A_1 = \frac{2}{\pi}\cos\left(v+\frac{1}{2}\right)\pi$.

(ii) When $l \neq 0$ (see Lebedev 1965, p. 172,199)

$$P_v^l(\cosh\alpha) = A_2\int_{-\alpha}^{\alpha} \frac{e^{-(v+\frac{1}{2})\theta}T_l(\cos\psi)}{\sqrt{2\cosh\alpha - 2\cosh\theta}}\,d\theta \tag{B 3}$$

where $A_2 = \frac{\Gamma(v+m+1)}{\pi\Gamma(v+1)}$, Γ is the gamma function and T_l is the Chebyshev polynomial.

Other functions used in Eq. (2.18) in the main text are

$$\frac{T_\alpha}{af} = \sinh\alpha\left(2\sin\beta_0\frac{a_1}{a}+\tau\frac{f_1}{f}\right)+b\left(2\sinh\alpha\left(\sin\beta_0\frac{a_2}{a}+\tau\frac{f_1}{f}\frac{a_1}{a}\right)\right) \tag{B 4}$$

$$\begin{aligned}\frac{T_{\alpha\alpha}}{af} = {} & 2\sin^2 h\alpha\left(2\sin\beta_0\frac{a_1}{a}+\tau\frac{f_1}{f}\right)+2\sin^2 h\alpha\left(2\sin\beta_0\frac{a_2}{a}+\tau\frac{f_1}{f}\frac{a_1}{a}\right)\\ & +4b\sinh^2\alpha\left(2\sin\beta_0\frac{a_3}{a}+\tau\frac{f_1}{f}\frac{a_2}{a}\right)+\cosh\alpha\left(2\sin\beta_0\frac{a_1}{a}+\tau\frac{f_1}{f}\right)\\ & +2b\cosh\alpha\left(2\sin\beta_0\frac{a_2}{a}+\tau\frac{f_1}{f}\frac{a_1}{a}\right)\end{aligned} \tag{B 5}$$

where notations $a_1 = 0.5/a$, $a_2 = -0.25/a^3$, $a_3 = 0.375/a^5$ and $f_1 = \cosh\tau\beta_0 - \coth\tau\pi\sinh\tau\beta_0$.

REFERENCES

Basaran, O. A. 1992 Nonlinear oscillations of viscous liquid drops. *J. Fluid Mech.* **241**, 169–198.

Bostwick, J. B. & Steen, P. H. 2014 Dynamics of sessile drops. Part 1. Inviscid theory. *J. Fluid Mech.* **760**, 5–38.

Bostwick, J. B. & Steen, P. H. 2015 Stability of constrained capillary surfaces. *Ann. Rev. of Fluid Mech.* **47**, 539–568.

Bostwick, J. B. & Steen, P. H. 2016 Response of driven sessile drops with contact-line dissipation. *Soft matter* **12** (43), 8919–8926.

Brunet, P. Eggers & J. Deegan, R. D. 2007 Vibration-induced climbing of drops. *Phys. Rev. Let.* **99** (14), 144501.

Chandrasekhar, S. 1959 The oscillations of a viscous liquid globe. *Proc. Lond. Math. Soc.* **3** (1), 141–149.

Chang, C. T., Bostwick, J. B., Daniel, S. & Steen, P. H. 2015 Dynamics of sessile drops. Part 2. Experiment. *J. Fluid Mech.* **768**, 442–467.

Chang, C. T., Bostwick, J. B., Steen, P. H. & Daniel, S. 2013 Substrate constraint modifies the rayleigh spectrum of vibrating sessile drops. *Phys. Rev. E* **88** (2), 023015.

Davis, S. H. 1980 Moving contact lines and rivulet instabilities. part 1. the static rivulet. *J. Fluid Mech.* **98** (2), 225–242.

Deserno, M. 2004 Notes on differential geometry. `https://www.cmu.edu/biolphys/deserno/pdf/diff_geom.pdf`.

Drazin, P. G. 2002 *Introduction to hydrodynamic stability*. Cambridge university press.

Fokas, A. S. & Nachbin, A. 2012 Water waves over a variable bottom: a non-local formulation and conformal mappings. *J. Fluid Mech.* **695**, 288.

Kreyszig, E. 1959 *Differential geometry*. University of Toronto Press.

Lamb, H. 1932 *Hydrodynamics*. Cambridge University Press.

Landau, L. D. & Lifshitz., E. M. 1987 *Fluid Mechanics, V. 6 of Course of Theoretical Physics*. Pergamon Press.

Lebedev, N. N. 1965 *Special Functions and their Applications.*. Prentice-Hall.

Li, T., Kar A. & Kumar, R. 2019 Marangoni circulation by uv light modulation on sessile drop for particle agglomeration. *J. Fluid Mech.* **873**, 72–88.

Lubarda, V. A. & Talke, K. A. 2011 Analysis of the equilibrium droplet shape based on an ellipsoidal droplet model. *Langmuir* **27** (17), 10705–10713.

Lyubimov, D. V., Lyubimova, T. P. & Shklyaev, S. V. 2006 Behavior of a drop on an oscillating solid plate. *Physics of Fluids* **18** (1), 012101.

Mettu, S. & Chaudhury, M. K. 2012 Vibration spectroscopy of a sessile drop and its contact line. *Langmuir* **28** (39), 14100–14106.

Miller, C.A. & Scriven, L.E. 1968 The oscillations of a fluid droplet immersed in another fluid. *J. Fluid Mech.* **32** (3), 417–435.

Noblin, X., Buguin, A. & Brochard-Wyart, F. 2004 Vibrated sessile drops: Transition between pinned and mobile contact line oscillations. *The Euro. Phys. J. E* **14** (4), 395–404.

Popov, Y. O. 2005 Evaporative deposition patterns: spatial dimensions of the deposit. *Phys. Rev. E* **71** (3), 036313.

Prosperetti, A. 1980 Normal-mode analysis for the oscillations of a viscous liquid drop in an immiscible liquid. *J. Fluid Mech.* **19** (3), 149–182.

Prosperetti, A. 2012 Linear oscillations of constrained drops, bubbles, and plane liquid surfaces. *Phys. Fluids* **24** (3), 032109.

Ramalingam, S., Ramkrishna, D. & Basaran, O. A. 2012 Free vibrations of a spherical drop constrained at an azimuth. *Phys. of Fluids* **24**, 082102.

Rayleigh, L. 1879 On the capillary phenomena of jets. *Proc. Roy. Soc. Lond.* **29** (196-199), 71–97.

Richardson, S. 1992 Hele-shaw flows with time-dependent free boundaries involving injection through slits. *Stud. in App. Math.* **87** (2), 175–194.

Shaikeea, A. J. D., Basu, S., Tyagi, A., Sharma, S., Hans, R. & Bansal, L. 2017 Universal representations of evaporation modes in sessile droplets. *PloS one* **12** (9), e0184997.

Sharp, J. S. 2012 Resonant properties of sessile droplets; contact angle dependence of the resonant frequency and width in glycerol/water mixtures. *Soft Matter* **8** (2), 399–407.

Steen, P. H., Chang, C. T. & Bostwick, J. B. 2016 Droplet motions fill a periodic table. *Proc. Nat. Acad. Sci.* **12** (43), 8919–8926.

Strani, M. & Sabetta, F. 1984 Free vibrations of a drop in partial contact with a solid support. *J. Fluid Mech.* **141**, 233–247.

Tsamopoulos, John A. & Brown, Robert A. 1983 Nonlinear oscillations of inviscid drops and bubbles. *J. Fluid Mech.* **127**, 519–537.

Wilkes, Edward D. & Basaran, Osman A. 1994 Nonlinear oscillations of pendant drops. *Phys. Fluids* **6** (9), 2923–2943.

Wilkes, Edward D. & Basaran, Osman A. 1997 Forced oscillations of pendant (sessile) drops. *Phys. Fluids* **9** (6), 1512–1528.

Wilkes, Edward D. & Basaran, Osman A. 2001 Drop ejection from an oscillating rod. *J. Colloidal Interface Sci.* **242**, 180–201.